Available online at www.sciencedirect.com
SCIENCE DIRECT®
Journal of Nuclear Materials 353 (2006) 52–65
journal of nuclear materials
www.elsevier.com/locate/jnucmat

Mechanism map for nucleation and growth of helium bubbles in metals

Kazunori Morishita [a,*], Ryuichiro Sugano [b]

[a] Institute of Advanced Energy, Kyoto University, Gokasho, Uji, Kyoto 611-0011, Japan
[b] Research Institute for Applied Mechanics, Kyushu University, Kasuga, Fukuoka 816-8580, Japan

Received 14 October 2005; accepted 5 March 2006

Abstract

The total free energy of a system containing helium bubbles and point defects (vacancies, helium and self-interstitial atoms) was evaluated and activation barrier for forming a helium bubble was derived, where the effect of helium on helium bubble formation is clearly shown. The rates of inflow to a helium bubble and outflow from a helium bubble were evaluated for vacancies, helium and self-interstitial atoms at the equilibrium and irradiation conditions to understand the mechanism of nucleation and growth of helium bubbles. It indicates that both the thermal emissions of helium and self-interstitial atoms may competitively occur at the irradiation condition from relatively small helium bubbles with high helium pressure.

PACS: 61.80.Az; 61.72.Cc; 61.72.Ji; 61.72.Qq

1. Introduction

In the fusion reactor environment, concurrently with atomic displacements, helium and hydrogen isotopes are introduced into fusion materials by direct implantation or by nuclear transmutation reactions during neutron irradiation, which can produce significant changes in material microstructure and properties, and moreover may cause even decisive damage to fusion plasma stability. Especially, high helium concentrations and the formation of helium bubbles in metals are known to enhance void swelling, produce surface roughening and blistering, and cause high temperature intergranular embrittlement. Therefore, precise understanding of helium behavior in metals still remains one of the most important subjects in the field of research and development of nuclear fusion reactor materials.

The theory of helium bubble formation has been developed by many researchers. Russell et al. [1–4] derived equations describing the absorption and emission rates of vacancies and helium atoms to and from a helium bubble, respectively, and they suggested the nucleation path of the helium bubble.

* Corresponding author. Tel.: +81 774 38 3477; fax: +81 774 38 3479.
E-mail address: morishita@iae.kyoto-u.ac.jp (K. Morishita).

0022-3115/$ - see front matter © 2006 Elsevier B.V. All rights reserved.
doi:10.1016/j.jnucmat.2006.03.007

Mansur et al. [5–7] and Stoller et al. [8,9] derived an equation to evaluate void growth rate using the rates of vacancy absorption, vacancy emission and self-interstitial atom (SIA) absorption, and they applied it to simultaneous rate theory equations for evaluation of helium-assisted void growth and accumulation. All these theoretical treatments are well established, available for relatively lower concentrations of helium in metals, and can be applied enough to modeling the behaviors of fusion structural materials under irradiation, where helium is produced by (n,α) nuclear reactions. However, these treatments are still insufficient to be applied to the problem of plasma–surface interaction (PSI) where helium concentration in plasma facing materials is expected to be much higher than that in the structural materials.

In plasma facing materials where helium atoms are directly implanted, the helium pressure of bubbles can be so high that the emissions of an SIA and its cluster from a helium bubble are greatly expected. In fact, experimental transmission electron microscopy (TEM) observation during helium implantation showed the production of SIA clusters (loops) that may be punched out from high pressure helium bubbles [10,11]. In addition, it is also expected that high pressure helium bubbles frequently emit helium atoms that play an important role on the thermal stability of helium bubbles. Although all the absorption and emission rates of vacancies, helium and SIAs are important factors for the nucleation and growth of helium bubbles, the rates of the SIA and helium emissions are not fully included in the models above. In the present study, all the point defect absorption and emission rates are incorporated into the model and the mechanism of nucleation and growth of helium bubbles in bcc Fe is investigated.

2. Theory

2.1. Total free energy of a system

The total free energy of a system containing various types of helium bubbles, isolated vacancies, isolated helium substitutional and isolated SIAs is given per a lattice site as follows:

$$g = \sum_j C^j_{\text{bubble}}\mu^j_{\text{bubble}} + C^{\text{matrix}}_{\text{subHe}}\mu^{\text{matrix}}_{\text{subHe}} + C^{\text{matrix}}_{\text{V}}\mu^{\text{matrix}}_{\text{V}} + C^{\text{matrix}}_{\text{SIA}}\mu^{\text{matrix}}_{\text{SIA}}, \quad (1)$$

where j indicates the type of helium bubbles, which is represented by the numbers of helium atoms (N^{b}_{He}) and vacancies (N^{b}_{V}) in a helium bubble. C^j_{bubble} and μ^j_{bubble} are the concentration and chemical potential of type j helium bubbles, respectively, and C^{matrix}_k and μ^{matrix}_k are the concentration and chemical potential of point defects in the matrix, respectively, where k indicates helium substitutional (subHe), vacancies (V) or SIAs (SIA). In the present study, defect concentrations are represented by the fraction of the number of defects to the number of lattice sites in the system considered. In addition, the entropy of a system described below is what is known as the configurational entropy.

2.2. Chemical potentials

The chemical potential of point defects in the matrix is represented by

$$\mu^{\text{matrix}}_k = E^{\text{f}}_k + k_{\text{B}}T\ln C^{\text{matrix}}_k, \quad (2)$$

where E^{f}_k is the formation energy of type k point defects in the matrix, and $k_{\text{B}}T$ has its usual meaning.

The chemical potential of type j helium bubbles can be written by the following two different forms. One is the same form as Eq. (2), which is given by

$$\mu^j_{\text{bubble}} = G^j_{\text{bubble}} + k_{\text{B}}T\ln C^j_{\text{bubble}}, \quad (3)$$

where G^j_{bubble} is the formation free energy of type j helium bubbles. The other form is obtained using the chemical potentials of point defects in helium bubbles, $\mu^{\text{b},j}_k$, where k denotes vacancies, helium or SIAs. When a helium bubble is constituted by m^j_{b} vacancies, n^j_{b} helium and l^j_{b} SIAs, the chemical potential of the helium bubble is written by the following form:

$$\mu^j_{\text{bubble}} = n^j_{\text{b}}\mu^{\text{b},j}_{\text{He}} + m^j_{\text{b}}\mu^{\text{b},j}_{\text{V}} + l^j_{\text{b}}\mu^{\text{b},j}_{\text{SIA}}, \quad (4)$$

where n^j_{b} is identical to N^{b}_{He} defined above. SIAs in helium bubbles are considered to be spontaneously recombined with vacancies at helium bubble surface, and therefore the physical meaning of 'an SIA in helium bubbles' indicates a lattice atom at helium bubble surface. Thus, m^j_{b} and l^j_{b} are reasonably considered to have the relation: $N^{\text{b},j}_{\text{V}} = m^j_{\text{b}} - l^j_{\text{b}}$, where m^j_{b} must be greater than l^j_{b} because of helium bubble size to be positive. It is emphasized here that introducing the chemical potential of SIAs in a helium bubble ($\mu^{\text{b},j}_{\text{SIA}}$) into Eq. (4) seems to be unusual and somewhat artificial, but it is significant for understanding the binding states between SIAs

and helium bubbles as shown below. Using the formation free energy of helium bubbles G^j_{bubble}, the chemical potentials of point defects in a helium bubble are written by

$$\begin{cases} \mu^{\text{b},j}_{\text{He}} = \dfrac{\partial G^j_{\text{bubble}}}{\partial n^j_{\text{b}}} = \dfrac{\partial G^j_{\text{bubble}}}{\partial N^{\text{b}}_{\text{He}}}, \\ \mu^{\text{b},j}_{\text{V}} = \dfrac{\partial G^j_{\text{bubble}}}{\partial m^j_{\text{b}}} = \dfrac{\partial G^j_{\text{bubble}}}{\partial N^{\text{b}}_{\text{V}}}, \\ \mu^{\text{b},j}_{\text{SIA}} = \dfrac{\partial G^j_{\text{bubble}}}{\partial l^j_{\text{b}}} = -\dfrac{\partial G^j_{\text{bubble}}}{\partial N^{\text{b}}_{\text{V}}}. \end{cases} \tag{5}$$

It is obvious from these equations that the chemical potential of vacancies in helium bubbles and that of SIAs in helium bubbles have the relation:

$$\mu^{\text{b},j}_{\text{V}} = -\mu^{\text{b},j}_{\text{SIA}}. \tag{6}$$

It indicates that a work done by introducing a vacancy into helium bubbles is equivalent to a work done by extracting an SIA (i.e., a lattice atom at helium bubble surface) from the helium bubbles.

2.3. Equilibrium condition

When a system is in equilibrium, the total free energy change must be 0 for any infinitesimal changes in the concentrations of point defects and helium bubbles in the system. Thus, from Eq. (1), we obtained the equilibrium condition of the system, as follows:

$$\begin{cases} \mu^{\text{b},j}_{\text{He}} - \mu^{\text{matrix}}_{\text{subHe}} + \mu^{\text{matrix}}_{\text{V}} = 0, \\ \mu^{\text{b},j}_{\text{V}} - \mu^{\text{matrix}}_{\text{V}} = 0, \\ \mu^{\text{b},j}_{\text{SIA}} - \mu^{\text{matrix}}_{\text{SIA}} = 0, \\ \mu^j_{\text{bubble}} - n^j_{\text{b}}\left(\mu^{\text{matrix}}_{\text{subHe}} - \mu^{\text{matrix}}_{\text{V}}\right) \\ \quad -m^j_{\text{b}}\mu^{\text{matrix}}_{\text{V}} - l^j_{\text{b}}\mu^{\text{matrix}}_{\text{SIA}} = 0. \end{cases} \tag{7}$$

Equations described here indicate equilibrium condition between a helium bubble and a matrix point defect. Using Eqs. (5) and (7), the chemical potentials of matrix point defects are given by

$$\begin{cases} \mu^{\text{matrix}}_{\text{subHe}} = \dfrac{\partial G^j_{\text{bubble}}}{\partial N^{\text{b}}_{\text{He}}} + \dfrac{\partial G^j_{\text{bubble}}}{\partial N^{\text{b}}_{\text{V}}}, \\ \mu^{\text{matrix}}_{\text{V}} = \dfrac{\partial G^j_{\text{bubble}}}{\partial N^{\text{b}}_{\text{V}}}, \\ \mu^{\text{matrix}}_{\text{SIA}} = -\dfrac{\partial G^j_{\text{bubble}}}{\partial N^{\text{b}}_{\text{V}}}, \\ \mu^j_{\text{bubble}} = N^{\text{b}}_{\text{He}}\dfrac{\partial G^j_{\text{bubble}}}{\partial N^{\text{b}}_{\text{He}}} + N^{\text{b}}_{\text{V}}\dfrac{\partial G^j_{\text{bubble}}}{\partial N^{\text{b}}_{\text{V}}}. \end{cases} \tag{8}$$

It is shown here that, similar to Eq. (6), the chemical potentials of vacancies and SIAs in the matrix have a relation:

$$\mu^{\text{matrix}}_{\text{V}} + \mu^{\text{matrix}}_{\text{SIA}} = 0. \tag{9}$$

It clearly indicates recombination reaction (V + SIA = 0) between vacancies and SIAs in the matrix in equilibrium with each other. In addition, when helium interstitial in the matrix is introduced into the system, the chemical potential of matrix helium interstitial is written by

$$\mu^{\text{matrix}}_{\text{intHe}} = \frac{\partial G^j_{\text{bubble}}}{\partial N^{\text{b}}_{\text{He}}}. \tag{10}$$

From Eqs. (8) and (10), the following relation is obtained:

$$\mu^{\text{matrix}}_{\text{subHe}} = \mu^{\text{matrix}}_{\text{intHe}} + \mu^{\text{matrix}}_{\text{V}}. \tag{11}$$

It clearly shows that helium substitutional in the matrix is in equilibrium with helium interstitial and vacancies in the matrix. It is noted that Eqs. (8) and (10) represent equilibrium conditions between a helium bubble and a matrix point defect, while Eqs. (9) and (11) show equilibrium condition among matrix point defects.

2.4. Binding free energy

In this section, the binding free energies of vacancies, helium and SIAs to a helium bubble are derived. The binding free energy of point defects to a helium bubble G^{bind}_k is defined as the energy which provides the concentration of matrix point defects in equilibrium with a helium bubble, where k denotes vacancies, helium, or SIAs:

$$C^{\text{matrix}}_k = \exp\left(-\frac{G^{\text{bind}}_k}{k_{\text{B}}T}\right). \tag{12}$$

Using Eqs. (2), (8), (10) and (12), the binding free energies of point defects to a helium bubble are obtained as follows:

$$\begin{cases} G^{\text{bind}}_{\text{subHe}} = E^{\text{f}}_{\text{subHe}} - \left(\dfrac{\partial G^{\text{j}}_{\text{bubble}}}{\partial N^{\text{b}}_{\text{He}}} + \dfrac{\partial G^{\text{j}}_{\text{bubble}}}{\partial N^{\text{b}}_{\text{V}}}\right), \\ G^{\text{bind}}_{\text{V}} = E^{\text{f}}_{\text{V}} - \dfrac{\partial G^{\text{j}}_{\text{bubble}}}{\partial N^{\text{b}}_{\text{V}}}, \\ G^{\text{bind}}_{\text{SIA}} = E^{\text{f}}_{\text{SIA}} + \dfrac{\partial G^{\text{j}}_{\text{bubble}}}{\partial N^{\text{b}}_{\text{V}}}, \\ G^{\text{bind}}_{\text{intHe}} = E^{\text{f}}_{\text{intHe}} - \dfrac{\partial G^{\text{j}}_{\text{bubble}}}{\partial N^{\text{b}}_{\text{He}}}. \end{cases} \tag{13}$$

Note that from Eq. (13) one obtains the equation: $G_{\mathrm{V}}^{\mathrm{bind}} + G_{\mathrm{SIA}}^{\mathrm{bind}} = E_{\mathrm{V}}^{\mathrm{f}} + E_{\mathrm{SIA}}^{\mathrm{f}}$. Since the right-hand side of this equation is considered to be a constant, the binding free energy of vacancies and that of SIAs have a trade-off relation with each other. Namely, when the vacancy binding free energy increases, the SIA binding free energy decreases, and vice versa.

When similar operations were applied to Eqs. (3) and (7), the following relation was obtained regarding the equilibrium concentration of helium bubbles:

$$C_{\mathrm{bubble}}^{j} = \exp\left(-\frac{G_{\mathrm{bubble}}^{\mathrm{bind},j}}{k_{\mathrm{B}}T}\right), \tag{14a}$$

$$G_{\mathrm{bubble}}^{\mathrm{bind},j} = G_{\mathrm{bubble}}^{j} - N_{\mathrm{He}}^{\mathrm{b},j}\mu_{\mathrm{subHe}}^{\mathrm{matrix}} - \left(N_{\mathrm{V}}^{\mathrm{b},j} - N_{\mathrm{He}}^{\mathrm{b},j}\right)\mu_{\mathrm{V}}^{\mathrm{matrix}}. \tag{14b}$$

By using Eq. (11), Eq. (14b) changes to

$$G_{\mathrm{bubble}}^{\mathrm{bind},j} = G_{\mathrm{bubble}}^{j} - N_{\mathrm{He}}^{\mathrm{b},j}\mu_{\mathrm{intHe}}^{\mathrm{matrix}} - N_{\mathrm{V}}^{\mathrm{b},j}\mu_{\mathrm{V}}^{\mathrm{matrix}}. \tag{14c}$$

$G_{\mathrm{bubble}}^{\mathrm{bind}}$ is hereafter called the total binding free energy of helium bubbles. This energy is usually appeared in the classical nucleation and growth theory of precipitates, which provides the state of clustering and the probabilities of critical nucleus production and embryo annihilation under the equilibrium condition.

2.5. Formation free energy of helium bubbles

The formation free energy of helium bubbles $G_{\mathrm{bubble}}^{j} = G_{\mathrm{bubble}}(N_{\mathrm{He}}^{\mathrm{b}}, N_{\mathrm{V}}^{\mathrm{b}})$ is defined as changes in system free energy when a helium bubble is introduced into a perfect crystal. Following the work done by Trinkaus [12], the formation free energy of helium bubbles is written as follows:

$$G_{\mathrm{bubble}} = G_{\mathrm{He}}^{\mathrm{Bulk}} + G_{\mathrm{He}}^{\mathrm{Surface}} + G_{\mathrm{Metal}}^{\mathrm{Surface}} + G_{\mathrm{He-Metal}}^{\mathrm{Interface}} + G_{\mathrm{relax}}, \tag{15}$$

where $G_{\mathrm{He}}^{\mathrm{Bulk}}$ is the bulk helium free energy, $G_{\mathrm{He}}^{\mathrm{Surface}}$ is the surface helium free energy, $G_{\mathrm{Metal}}^{\mathrm{Surface}}$ is the metal surface free energy, $G_{\mathrm{He-Metal}}^{\mathrm{Interface}}$ is the interface free energy between metal matrix and helium, and G_{relax} is the relaxation free energy. The respective terms of the formation free energy can be described in the following, when it is assumed that a helium bubble has a spherical shape with a radius of R in bcc Fe matrix.

The bulk helium energy $G_{\mathrm{He}}^{\mathrm{Bulk}}$ due to $N_{\mathrm{He}}^{\mathrm{b}}$ helium atoms was calculated using the helium equation of states (EOS) and the following relation obtained from the Gibbs–Duhem relation at constant temperature.

$$G_{\mathrm{He}}^{\mathrm{Bulk}}(p) = G_{\mathrm{He}}^{\mathrm{Bulk}}(p_0) + \int_{p_0}^{p} V(p)\mathrm{d}p,$$

where V is the volume containing $N_{\mathrm{He}}^{\mathrm{b}}$ helium, p is helium pressure, and p_0 is reference pressure. If the reference pressure is small enough to consider helium state as ideal gas, $G_{\mathrm{He}}^{\mathrm{Bulk}}(p_0)$ can be evaluated using the statistical thermodynamics.

In order to describe the state of fluid helium appropriately in wide pressure ranges, three different forms of EOSs published in literatures were connected using two different interpolation functions, as follows:

$$v_{\mathrm{m}}^{\mathrm{Fluid}}(p) = \begin{cases} v_{\mathrm{m}}^{\mathrm{ideal}}(p) \cdots p \leqslant p_1, \\ v_{\mathrm{m}}^{\mathrm{interpolate1}}(p) \cdots p_1 \leqslant p \leqslant p_2, \\ v_{\mathrm{m}}^{\mathrm{CS}}(p) \cdots p_2 \leqslant p \leqslant p_3, \\ v_{\mathrm{m}}^{\mathrm{interpolate2}}(p) \cdots p_3 \leqslant p \leqslant p_4, \\ v_{\mathrm{m}}^{\mathrm{MLB}}(p) \cdots p_4 \leqslant p, \end{cases}$$

where $p_1 = 0.5 \times 10^5$ Pa, $p_2 = 10^6$ Pa, $p_3 = 10^8$ Pa and $p_4 = 2 \times 10^8$ Pa. The superscripts ideal, CS and MLB indicate the EOS of ideal helium gas, the EOS developed by Brearley and MacInnes [13], and the EOS developed by Mills et al. [14], respectively. The superscripts interpolate1 and interpolate2 indicate the interpolation function of type 1 which connects the ideal and CS EOSs and the interpolation function of type 2 which connects the CS and MLB EOSs, respectively. The virial EOS was employed as the interpolation functions, where the compressibility factor of helium was described in the form of a polynomial function of pressure,

$$z = \frac{pv_{\mathrm{m}}}{k_{\mathrm{B}}T} = b_0 + b_1 p + b_2 p^2 + b_3 p^3.$$

The virial coefficients b_k for the interpolation function of type 1 were determined so as to fit the compressibility factor and its pressure derivative to those of ideal gas at pressure p_1 and to those of CS EOS at pressure p_2. The virial coefficients for the interpolation function of type 2 were also obtained in the same way as those of the type 1, using the compressibility factors and their pressure derivatives at p_3 and p_4. Note that, the virial coefficients b_k thus obtained depend on temperature.

For description of the state of solid helium, on the other hand, the Vinet EOS [15] developed by Zha et al. [16] was employed in the present study.

The coefficients for giving the Debye temperature and the Gruneisen parameter required for use of the EOS were modified in the present study using helium density data of Driessen and van der Poll [17] as well as those of Zha et al. [16], for the EOS to be available in wider helium density ranges.

In the choice of fluid EOS or solid EOS, the melting curve of helium in the form of the Kechin equation [18] was employed. In the present study, in order to obtain melting curve to be available in wider temperature ranges (300–1000 K), the parameters required in the equation were also modified to fit the $P_m - T_m$ data of Driessen and van der Poll [17], Datchi et al. [19] and Young et al. [20]. Note that Young's data were derived by theoretical LMTO calculations.

The surface helium energy $G_{He}^{Surface}$ is considered to be a correction term to the bulk helium energy G_{He}^{Bulk} due to the deficit of He–He bonds at helium bubble surface. The following form was used here:

$$G_{He}^{Surface} = -f\left(N_{He}^{b}\right)^{-1/3} G_{He}^{Bulk}, \tag{16}$$

where f is a constant which represents the fraction of the number of deficit of He–He bonds at the surface to the number of He–He bonds per a helium atom without any deficit. Fujita [21] actually counted the numbers of the deficit of the bonds for a spherical fcc cluster and evaluated that f approaches 1.37 with increasing cluster size, while Trinkaus [12] estimated using the volume and surface area of spheres that f is about 0.6. The difference between their values may be negligible, compared to the total estimation of Eq. (15). In the present study, $f = 1.37$ was employed.

The metal surface free energy $G_{Metal}^{Surface}$ employed here has the form of

$$G_{Metal}^{Surface} = \gamma S\left(1 - \frac{q}{R}\right), \tag{17}$$

where γ is the surface free energy of metal flat surface, S is the surface area of a spherical helium bubble, and q is a constant value. The second term of Eq. (17) represents curvature correction to the first term, and it converges to 0 for large R. In the present study, the parameters, γ and q, were obtained by fitting the formation energy of unrelaxed voids in bcc Fe, which were calculated using the Ackland Fe–Fe interatomic potentials [22]. A least square fitting to the calculated formation energy provided $\gamma = 1.195 \times 10^{19}$ eV/m^2 and $q = 5.194 \times 10^{-11}$ m.

Let us define G_{bubble}^{0} by the following equation:

$$G_{bubble}^{0} = G_{He}^{Bulk} + G_{He}^{Surface} + G_{Metal}^{Surface}.$$

It is considered that principal contributions to the formation free energy of helium bubbles can be expressed by G_{bubble}^{0}. However, additional two contributions to correct G_{bubble}^{0} must be considered as mentioned below: one is the correction of volume available for helium in a helium bubble due to high repulsive interaction between matrix metal atoms and helium, and the other is the correction of helium bubble volume due to the structural relaxation of a helium bubble.

So far, the volume available for helium in a helium bubble has been considered to be the same as helium bubble volume defined by $N_V^b\Omega$, where Ω is atomic volume. As pointed out in our previous work [23–26], however, metal–helium repulsive interaction is much greater than helium–helium repulsive one. Therefore, such a great difference of the repulsive interactions will reduce volume available for helium in a helium bubble, which leads to an increase of the bulk helium free energy. Trinkaus [12] assumed that a change in the radius of a sphere due to repulsive metal–helium interaction is a constant $-\delta_{He}$ and evaluated the free energy change as $F_{He-Metal}^{Interface} = p\delta_{He}S$, where $\delta_{He} \approx 0.1$ nm for helium in Ni. Following the Trinkaus model, we obtained here the energy change as

$$G_{He-Metal}^{Interface} = \left(\frac{\partial G_{He}^{Bulk}}{\partial V}\right)\delta_{He}S = B_T\delta_{He}S, \tag{18}$$

where B_T is helium bulk modulus. A difference between the Trinkaus expression and ours, i.e., p and B_T, is caused by a difference in the definition of free energy. Namely, Trinkaus used the Helmholtz free energy, while we adopted the Gibbs free energy. It is noted that, when helium is regarded as ideal gas, these expressions become exactly the same because helium bulk modulus for ideal gas is identical to helium pressure. The constant value δ_{He} was here fixed to be 0.04 nm for helium in bcc Fe, by fitting G_{bubble} to the formation energy of the helium bubbles of 20 vacancies that were calculated by MD techniques [23–26].

In addition, it has been so far assumed that helium bubble volume is fixed at $N_V^b\Omega$. However, helium bubble volume is considered to be increased due to helium pressure, leading to a decrease in the bulk helium energy, an increase in the surface

energies, and an introduction of the elastic energy of metal matrix. When the volume of a helium bubble is changed by δV, the formation free energy of helium bubbles can be written by

$$G_{\text{bubble}} = G^0_{\text{bubble}} + \left(\frac{\partial G^0_{\text{bubble}}}{\partial V}\right)\delta V + \frac{2\mu(1+\nu)}{9(1-\nu)}\frac{\delta V^2}{V}, \tag{19}$$

where ν is Poisson ratio and μ is the shear modulus of metal matrix. The last term is the elastic energy [27]. The relaxation volume δV was determined by minimizing G_{bubble} in this equation, and then the relaxation free energy was obtained as follows.

$$G_{\text{relax}} = -\frac{9V(1-\nu)}{8\mu(1+\nu)}\left(\frac{\partial G^{\text{o}}_{\text{bubble}}}{\partial V}\right)^2.$$

Using Eqs. (16)–(19), Eq. (15) finally becomes

$$G_{\text{bubble}} = \left(1 - \frac{f}{\left(N^{\text{b}}_{\text{He}}\right)^{1/3}}\right)G^{\text{Bulk}}_{\text{He}} + \gamma S\left(1 - \frac{q}{R}\right) + B_{\text{T}}\delta_{\text{He}}S - \frac{9V(1-\nu)}{8\mu(1+\nu)} \times \left\{\frac{2\gamma}{R} - \frac{q\gamma}{R^2} - \left(1 - \frac{f}{\left(N^{\text{b}}_{\text{He}}\right)^{1/3}}\right)B_{\text{T}}\right\}^2.$$

2.6. Steady-state nucleation and growth of helium bubbles

Let us consider the steady-state nucleation of helium bubbles [28]. When the effect of stress-induced defect diffusion due to lattice relaxation around a helium bubble is neglected, namely, when the defect capture efficiency of helium bubbles is assumed to be fixed at 1, the total currents (flux) of point defects to a spherical helium bubble is written by

$$J^{\text{net}}_k = J^{\text{IN}}_k - J^{\text{OUT}}_k = \frac{4\pi R}{\Omega}D_k(C_k(\infty) - C_k(R)), \tag{20}$$

where D_k is the diffusion coefficient of point defects k, and R is helium bubble radius. J^{IN}_k and J^{OUT}_k are the rates of inflow to a helium bubble and outflow from a helium bubble, respectively. $C_k(R)$ and $C_k(\infty)$ are the concentrations of matrix point defect k at R and at infinity from a helium bubble center, respectively. The outflow (thermal emission) rate is generally evaluated by assuming that point defects near a helium bubble are locally equilibrated with the helium bubble. Therefore, $C_k(R)$ is given by point defect binding energies defined by Eqs. (12) and (13). On the other hand, $C_k(\infty)$ is determined by the condition of whole the system considered. In the case of the equilibrium, Eqs. (9) and (11) are used to obtain $C_k(\infty)$, while in the case of irradiation condition where matrix point defects are not equilibrated with each other, $C_k(\infty)$ is usually provided by solving the simultaneous rate theory equations describing all defect interactions occurred in materials, such as the production, annihilation, recombination and clustering of point defects.

3. Analysis

In order to investigate the mechanism of the nucleation and growth of helium bubbles in bcc Fe, the binding free energy of point defects to a helium bubble, the total binding free energy of helium bubbles, and the rates of inflow to a helium bubble and outflow from a helium bubble were evaluated.

The binding free energies of vacancies, helium and SIAs were obtained by Eq. (13) as a function of the numbers of helium atoms and vacancies in a helium bubble, $(N^{\text{b}}_{\text{He}}, N^{\text{b}}_{\text{V}})$.

The total binding free energy of helium bubbles given by Eq. (14) was obtained by following three steps: Firstly, total defect concentrations were given as input parameters: X_{V} for vacancies, X_{He} for helium and X_{SIA} for SIAs, where *total* defect concentration means the fraction per a lattice site of the number of point defects introduced into the system, irrespective of whether they are in the form of isolated defects or clustered defects. Then, the equilibrium concentrations of matrix point defects and helium bubbles were obtained at a given temperature by simultaneously solving Eqs. (8)–(11) using the parameters (X_{V}, X_{He}, X_{SIA}). Finally, the total binding free energy of helium bubbles was obtained as a function of $(N^{\text{b}}_{\text{He}}, N^{\text{b}}_{\text{V}})$.

The inflow and outflow rates of point defects during the steady-state nucleation and growth of helium bubbles were evaluated using Eq. (20). The concentration of type k point defects at R denoted by $C_k(R)$ was provided by Eq. (12) as a function of $(N^{\text{b}}_{\text{He}}, N^{\text{b}}_{\text{V}})$, while $C_k(\infty)$ was given depending on the following two conditions. One is the equilibrium condition, where a helium bubble and matrix point defects are in equilibrium with each other. This condition is considered to be an approximation to post-irradiation annealing condition. In this case, all Eqs. (8)–(11) were simultaneously solved to obtain $C_k(\infty)$. The other condition is the irradiation

condition where matrix point defects are not in equilibrium with each other. In the present study, $C_k(\infty)$ was regarded as fixed input parameters that are also depicted by (X_V, X_{He}, X_{SIA}) in the following.

4. Results and discussion

4.1. Point defect binding free energy

The binding free energies of vacancies, helium interstitials and SIAs to a helium bubble in bcc Fe were calculated using Eq. (13) as shown in Fig. 1(a), where the point defect binding free energy is plotted as a function of helium-to-vacancy ratio (He/V). The ratio is defined as the number of helium atoms in a helium bubble divided by the number of vacancies in a helium bubble, which is an indication of helium pressure of the helium bubble. The numbers of helium atoms and vacancies in a helium bubble that were used for the calculations range from 0 to 1100 and from 1 to 4080, respectively. The results for the helium bubbles of He/V ratios greater than 3 are omitted from the figure. Note that, minimum He/V ratios available for the evaluations become higher when helium bubble size becomes smaller. For example, a minimum He/V ratio for the helium bubble of 10 vacancies cannot take less than 0.1, while a He/V ratio for the helium bubble of 100 vacancies can take 0.01. As shown in the figure, for relatively smaller He/V ratios, vacancy binding energy is an increasing function of He/V ratios, while the helium and SIA binding energies are decreasing functions of the ratios. For He/V ratios greater than about 1.8, the reverse tendency is observed, where vacancy binding energy is a decreasing, and the helium and SIA binding energies are increasing functions. Moreover, for He/V ratios greater than about 2, these binding energies begin to vibrate with increasing the ratios. The vibrating behaviors may reflect the limitation of the linear elasticity theory that was applied for evaluation of the elastic and relaxation energies. It is therefore considered that the application range of the present analysis is limited for He/V ratios less than 2.

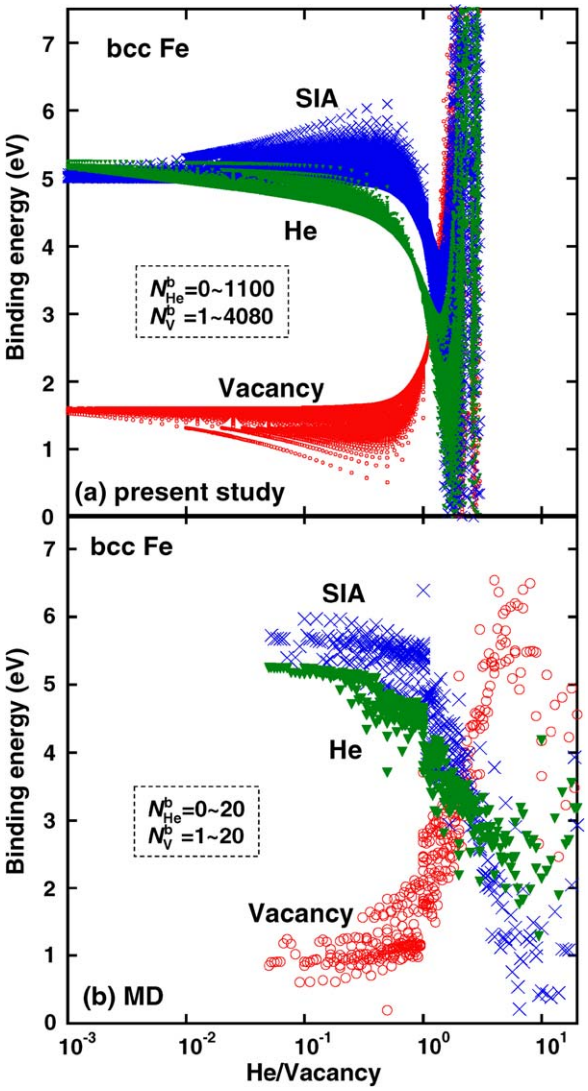

Fig. 1. (a) The point defect binding free energy of helium bubbles in bcc Fe for a vacancy, helium and SIAs obtained in the present study, and (b) the point defect binding energies obtained by our previous MD work [23–26].

Fig. 1(b) shows the point defect binding energies that we have evaluated for smaller size helium bubbles in bcc Fe using the MD technique with empirical interatomic potentials, where the trade-off relation of binding energies between vacancies and SIAs is also shown. The details were already described in [23–26]. In these results, the reverse tendency was appeared at the ratio of about 6, although it is much greater than the present value 1.8. This difference of critical ratios between the two evaluation methods is due to a difference in evaluation of lattice relaxations around a helium bubble. The plastic deformation of the matrix around a helium bubble was permitted by the MD technique, while it was not incorporated into the present analysis. Moreover, the MD results [23–26] showed the inhomogeneous displacement of matrix Fe atoms due to high helium pressure, while the

present analysis only permitted the uniform displacements of matrix Fe atoms that are distributed over the bubble–matrix interface within the application limit of the linear elasticity theory. Thus, the present analysis is inadequate for modeling the matrix Fe displacements around a helium bubble; nevertheless, it can be said that the dependence of the point defect binding energy on He/V ratios obtained in the present study for ratios less than about 2 is very similar to the MD results, and therefore, qualitative pictures described below is considered to be correct.

4.2. Total binding free energy of empty voids: temperature dependence

The total binding free energy of helium bubbles was defined by Eqs. (14b) and (14c), which is an indication of how many and how large precipitates will be produced under the equilibrium condition through Eq. (14a). In the present and following sections, the temperature and concentration dependence of the total binding free energy is shown to understand the characteristic of this energy.

Fig. 2 shows the total binding free energy of empty voids (without helium) as a function of temperature. Here, total vacancy concentration in the system X_V is fixed at 5×10^{-7}. The figure indicates that, with increasing the number of vacancies in an empty void (i.e., void size), the total binding free energy firstly increase, followed by a decrease. The maximum energy shows an activation barrier for forming a void nucleus, and it increases with increasing temperature.

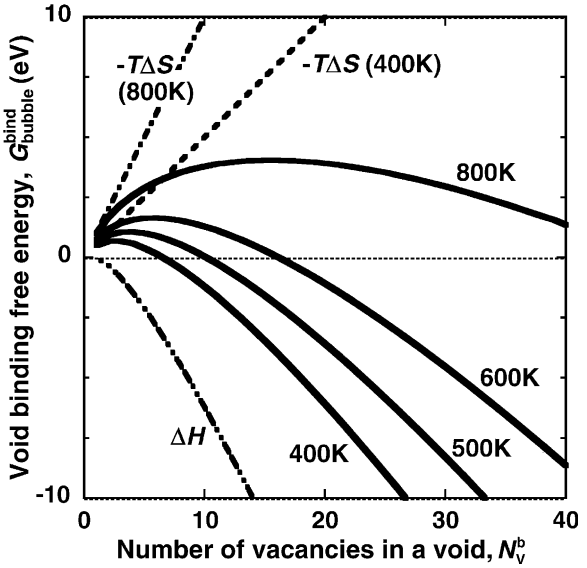

Fig. 2. Size dependence of the total binding free energy of empty voids in bcc Fe as a function of temperature. An activation barrier for forming a void nucleus increases with temperature.

In order to profoundly elucidate the temperature dependence of void nucleation, Eq. (14b) is divided into two terms such as $G^{\mathrm{bind},j}_{\mathrm{bubble}} = \Delta H - T\Delta S$ in the similar way to Refs. [29,30]. The former parameter ΔH is called an enthalpy term for void formation and the latter parameter $-T\Delta S$ is called an entropy term. Those parameters are expressed as follows:

$$\Delta H = G^{j}_{\mathrm{bubble}} - N^{\mathrm{b},j}_{\mathrm{He}} E^{\mathrm{f}}_{\mathrm{subHe}} - \left(N^{\mathrm{b},j}_{\mathrm{V}} - N^{\mathrm{b},j}_{\mathrm{He}}\right) E^{\mathrm{f}}_{\mathrm{V}},$$

$$-T\Delta S = -N^{\mathrm{b},j}_{\mathrm{He}} k_{\mathrm{B}} T \ln C^{\mathrm{matrix}}_{\mathrm{subHe}} - \left(N^{\mathrm{b},j}_{\mathrm{V}} - N^{\mathrm{b},j}_{\mathrm{He}}\right) k_{\mathrm{B}} T \ln C^{\mathrm{matrix}}_{\mathrm{V}}.$$

As shown in the figure, the enthalpy term ΔH is a monotonic decreasing function of void size, while the entropy term $-T\Delta S$ increases with increasing void size. The sum of the two terms produces the void size dependence of the total binding free energy mentioned above. The maximum of the total binding free energy corresponds to a critical size for void nucleation. As shown by the broken lines in the figure, the enthalpy term does not depend on temperature, while the entropy term significantly depends on temperature. Thus the temperature dependence of the activation barrier for forming a void nucleus is completely determined by the temperature dependence of the entropy term.

Such a temperature dependence of the activation barrier indicates that void nucleation becomes more difficult at higher temperature, and moreover, this is a reason why there exists a maximum temperature limit in which voids can form. The maximum temperature limit is what is called the stage V. Fig. 3(a) shows the temperature dependence of void nucleation rates defined by

$$J = J^{\mathrm{IN}}_{k} C^{*}_{\mathrm{void}} = J^{\mathrm{OUT}}_{k} C^{*}_{\mathrm{void}}.$$

Here, C^{*}_{void} is the concentration of critical void nuclei, which is calculated using Eq. (14a). Inflow and outflow rates denoted by J^{IN}_{k} and J^{OUT}_{k}, respectively, were calculated using Eq. (20). The vacancy migration energy was changed here as an input parameter ranging from 0.55 to 1.4 eV. Fig. 3(b) shows the temperature dependence of critical void nucleus concentrations and that of vacancy jump frequencies as a function of the vacancy migration energy. As shown in the figure, lower temperature limit for void formation is determined by the temperature dependence of vacancy jump frequencies,

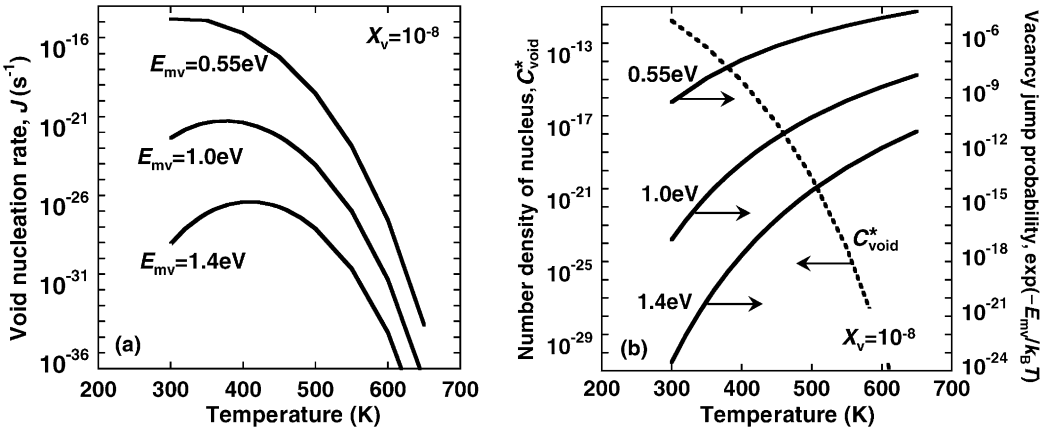

Fig. 3. Temperature dependence of (a) void nucleation rates, (b) critical void nucleus concentration and vacancy jump frequencies, as a function of vacancy migration energy. Voids can nucleate in limited temperature rages.

while higher temperature limit for void formation is determined by the temperature dependence of critical void nucleus formation as mentioned above.

4.3. Total binding free energy of empty voids: vacancy concentration dependence

Fig. 4 shows the total binding free energy of empty voids (without helium) at 500 K as a function of vacancy concentration. The enthalpy term does not depend on the vacancy concentration. However, the entropy term decreases with increasing the vacancy concentration. Therefore, the activation energy for forming a void nucleus decreases with increasing the vacancy concentration. It indicates that higher vacancy concentration will produce the higher probability of void formation.

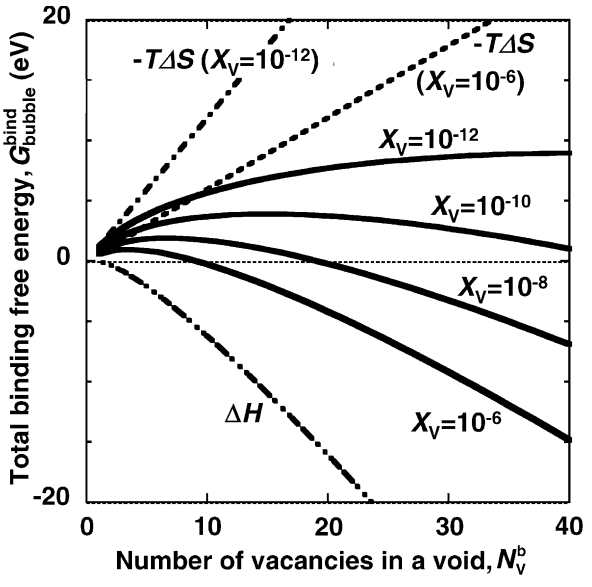

Fig. 4. Dependence of the total binding free energy of empty voids in bcc Fe on matrix vacancy concentration at 500 K. An activation barrier for forming a void nucleus increases with decreasing the vacancy concentration.

4.4. Total binding free energy of helium bubbles: helium effect

Fig. 5 shows the total binding free energy of helium bubbles at 800 K as a function of the

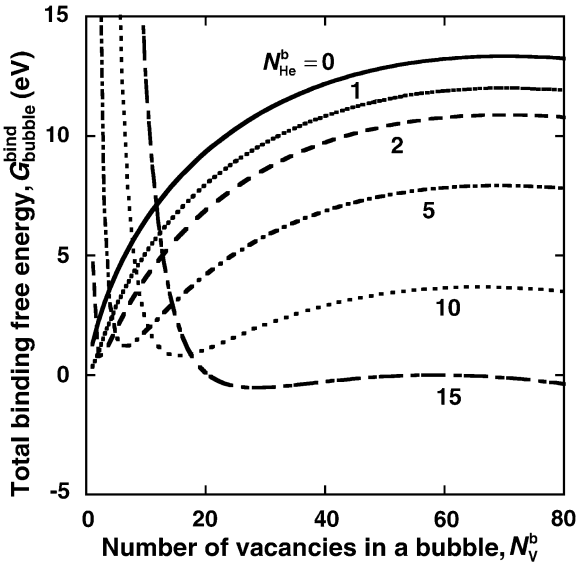

Fig. 5. Total binding free energy of helium bubbles in bcc Fe at 800 K as a function of the number of helium atoms in a helium bubble. Total defect concentrations in the system are $X_V = 10^{-8}$, $X_{He} = 10^{-10}$, $X_{SIA} = 6 \times 10^{-11}$. Significant reduction in an activation barrier for forming a helium bubble nucleus is caused by the introduction of helium.

number of helium atoms in a helium bubble N^{b}_{He}. Total defect concentrations in the system are $X_V = 10^{-8}$, $X_{He} = 10^{-10}$, $X_{SIA} = 6 \times 10^{-11}$. The contour plot representation of the total binding free energy is shown in Fig. 6, where the data for He/V ratios greater than 2 are omitted because of the application limit of the linear elasticity theory, as mentioned in Section 4.1. Temperature is so high and the total vacancy concentration is not so high (just about 500 times as many as the equilibrium vacancy concentration at this temperature), and therefore, the activation energy of empty voids is so large that voids cannot be expected to form. The activation energy is more than 10 eV, and the critical size of void nucleation is as high as 70 vacancies.

It can be mentioned from Eqs. (14b) and (2) that the introduction of helium into an empty void may increase the entropy term of the total binding free energy of helium bubbles. Simultaneously, however, it may significantly decrease the enthalpy term. The significant decrease in the enthalpy term sufficiently cancels the increase in the entropy term, and overall it results in a decrease in the total binding free energy. In fact, as shown in the figures, the activation barrier rapidly decreases with increasing the number of helium atoms in a helium bubble. The significant decrease in the enthalpy term is caused by the fact that, as pointed out in the previous MD work [23–26], the repulsive interaction between Fe and He is much greater than the relatively weak He–He interaction of a closed noble gas, and thus the energetically favorable helium clustering in Fe occurs through a decrease in the number of high energy, repulsive Fe–He interactions. As shown in the figures, the significant decrease in the total binding free energy by the introduction of helium finally leads to the disappearance of the activation barrier when the number of helium atoms in a helium bubble is greater than 17. This dramatic reduction in the activation barrier is an important role of helium on the formation of vacancy agglomerations.

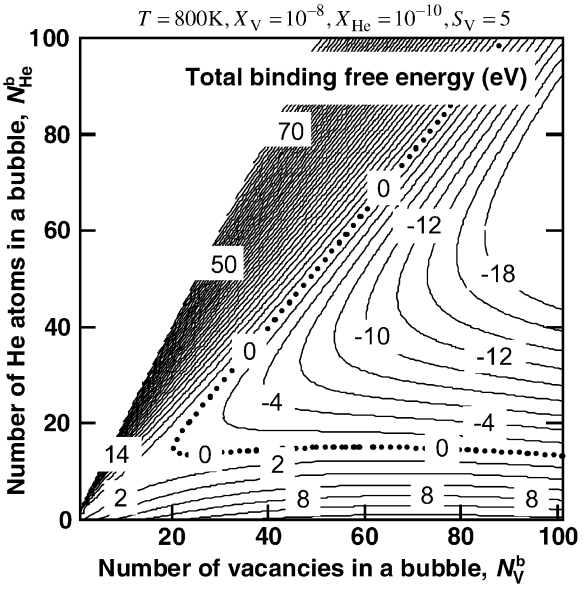

Fig. 6. A contour plot representation of the total binding free energy as a function of the numbers of helium atoms and vacancies in a helium bubble in bcc Fe at 800 K. Total defect concentrations in the system are $X_V = 10^{-8}$, $X_{He} = 10^{-10}$, $X_{SIA} = 6 \times 10^{-11}$.

Additional significant changes in the total binding free energy due to an introduction of helium into a helium bubble are clearly seen at the relatively smaller size, where the total binding free energy increases significantly with increasing the number of helium atoms in a helium bubble. This is because of a significant increase in the formation free energy of helium bubbles G^{j}_{bubble} due to high helium pressure. This significant increase in the total binding free energy at smaller size region results in the appearance of local minimum in the figure. With further increase in the number of helium atoms in a helium bubble, the local maximum and minimum values approach each other and finally the total binding free energy of helium bubbles shows a monotonic decreasing function of helium bubble size.

4.5. Helium bubble growth and shrinkage during post-irradiation annealing

The growth and shrinkage behavior of helium bubbles during post-irradiation annealing was investigated at the same condition as the previous section ($X_V = 10^{-8}$, $X_{He} = 10^{-10}$, $X_{SIA} = 6 \times 10^{-11}$, 800 K). The rates of inflow to a helium bubble and outflow from a helium bubble for vacancies, helium and SIAs were separately calculated as a function of the numbers of helium atoms and vacancies in a helium bubble, $(N^{b,j}_{He}, N^{b,j}_{V})$, using Eq. (20). Since matrix point defects and helium bubbles are considered to be in equilibrium with each other at this condition, their concentrations were obtained by simultaneously solving Eq. (7) and they were introduced into $C_k(\infty)$ in Eq. (20). This condition is hereafter called the equilibrium condition. Helium bubbles may grow by vacancy inflow and SIA outflow, while they may shrink by vacancy outflow

and SIA inflow, and therefore the growth rate J_{grow} and shrinkage rate J_{shrink} of helium bubbles were evaluated using the following equations:

$$J_{\text{grow}} = J_{\text{V}}^{\text{IN}} + J_{\text{SIA}}^{\text{OUT}},$$
$$J_{\text{shrink}} = J_{\text{V}}^{\text{OUT}} + J_{\text{SIA}}^{\text{IN}}.$$

Fig. 7 shows the contour map representation of the values of $\log_{10}(J_{\text{grow}}/J_{\text{shrink}})$ as a function of $(N_{\text{He}}^{\text{b},j}, N_{\text{V}}^{\text{b},j})$. The height 0 indicates that the rate of bubble growth is the same as that of bubble shrinkage, which is exhibited by a broken line in the map. Below the broken line helium bubbles will shrink and above the line helium bubbles will grow.

The broken line (the 0 height line) intersects the $N_{\text{He}}^{\text{b}} = 0$ line (it shows an empty void) at $N_{\text{V}}^{\text{b}} \approx 70$. It indicates that larger empty voids will grow and smaller empty voids will shrink than $N_{\text{V}}^{\text{b}} \approx 70$. This critical number is exactly the same as the critical number of vacancies in Fig. 5 that gives the maximum of the total binding free energy of empty voids. It indicates that the maximum value in Fig. 5 actually represents an activation barrier and the value $N_{\text{V}}^{\text{b}} \approx 70$ really shows a critical size for void nucleation at this condition. On the other hand, when N_{He}^{b} is greater than 2 and less than 18, the horizontal line of $N_{\text{He}}^{\text{b}} = \text{const.}$ intersects the broken line (the 0 height line) at two different N_{V}^{b} values in Fig. 7. The larger value corresponds to the local maximum of the total binding free energy of helium bubbles in Fig. 5, and the smaller value corresponds to the local minimum in the figure. Thus, the growth and shrinkage behaviors under the equilibrium condition strongly reflect the total binding free energy curve shown in Fig. 5.

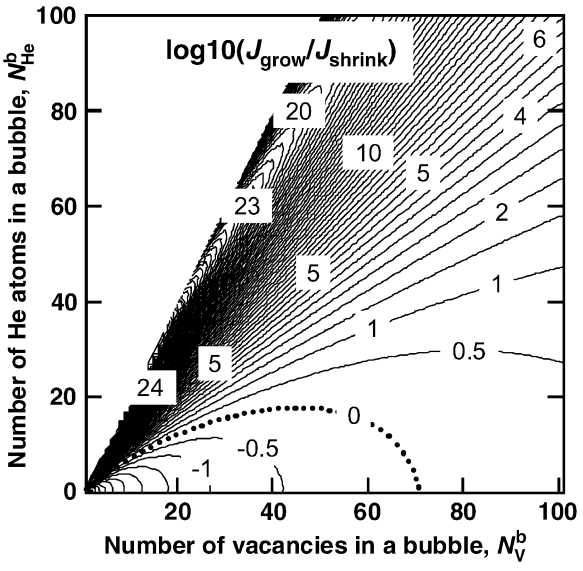

Fig. 7. A contour plot representing the growth (J_{grow}) and shrinkage (J_{shrink}) rates of helium bubbles in bcc Fe. The height of the contour is evaluated by $\log_{10}(J_{\text{grow}}/J_{\text{shrink}})$, and 0 height indicates that the growth rate equals to the shrinkage rate. Helium bubbles will grow and shrink in the positive and negative regions, respectively.

When the growth and shrinkage behaviors of helium bubbles were closely investigated, it was found that, below the broken line (the 0 height line), the rate of vacancy inflow is less than that of vacancy outflow, and the rate of SIA inflow is more than that of SIA outflow. In addition, above the broken line, the rate of vacancy inflow is more than that of vacancy outflow, and the rate of SIA inflow is less than that of SIA outflow. Furthermore, the region where the rate of vacancy inflow equals to the rate of vacancy outflow is identical to the region where the rates of SIA inflow and outflow equals to each other, and such the region is exactly identical to the broken line where the growth rate equals to the shrinkage rate. These symmetric behaviors of flow rates between vacancies and SIAs under the equilibrium condition are reflected by the fact that the chemical potentials of vacancies and SIAs in the matrix have such relationship as $\mu_{\text{V}}^{\text{matrix}} = -\mu_{\text{SIA}}^{\text{matrix}}$ under the equilibrium condition.

A further close investigation was made to find more dominant process for the growth and shrinkage; vacancy flow or SIA flow. In addition, the rates of helium inflow and outflow was also investigated as a function of $(N_{\text{He}}^{\text{b}}, N_{\text{V}}^{\text{b}})$, and it was found that helium outflow rate is greater than helium inflow rate when He/V ratios are greater than 0.65, while, otherwise, helium inflow rate is greater than helium outflow rate. From all the flow rates thus investigated, we finally obtained Fig. 8, which exhibits the mechanism of helium bubble nucleation and growth and is hereafter called *a mechanism map*. From the mechanism map, four regions are separately defined as follows: (A) the region where helium bubbles may shrink mainly by thermal vacancy emission (outflow) and helium may be absorbed, (B) the region where helium bubbles may grow mainly by vacancy absorption (inflow) and helium may be absorbed, (C) the region where helium bubbles may grow mainly by vacancy absorption and helium may be emitted, and (D) the region where helium bubbles may grow mainly by thermal SIA emission and helium may be emitted.

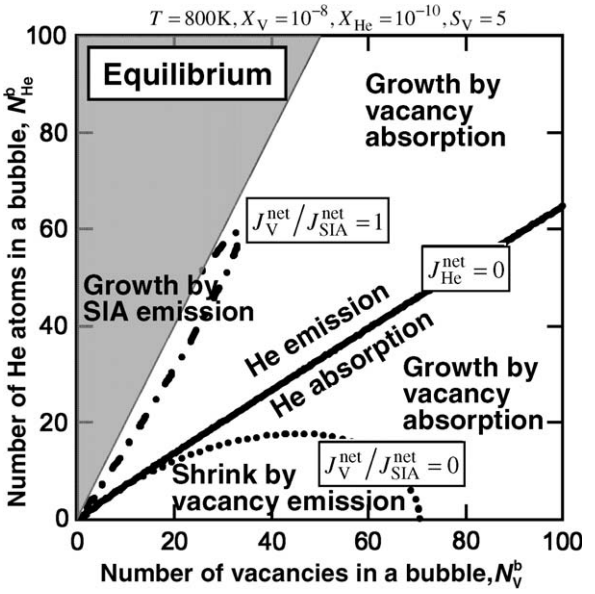

Fig. 8. A mechanism map for helium bubble nucleation and growth at the equilibrium condition at 800 K. Total defect concentrations are $X_V = 10^{-8}$, $X_{He} = 10^{-10}$, $X_{SIA} = 6 \times 10^{-11}$.

This mechanism map will provide a profound insight into helium bubble nucleation and growth at the equilibrium condition. The helium bubbles in the region (A) decrease N_V^b and increase N_{He}^b, and therefore, they will go in an upper left direction in Fig. 8. In the same way, the helium bubbles in the regions (B), (C) and (D) will go in an upper right direction, in a lower right direction, and again in a lower right direction, respectively. These qualitative but meaningful discussion on helium bubble growth and shrinkage involving helium desorption and absorption, will lead to useful suggestion that helium bubbles can grow firstly along a path where the $J_V^{net} = J_{SIA}^{net} = 0$ and $J_{He}^{net} = 0$ lines overlap with each other in Fig. 8. And then, after passing through the point $(N_{He}^b \approx 8, N_V^b \approx 10)$ where the two lines begin to separate, helium bubbles may grow in considerably wider regions in the map. The actual nucleation path of helium bubbles after passing this point may depend on a balance among point defect flow rates. This nucleation path is in well consistent with the earlier work done by Russell et al. [1–4].

Our model reveals the region (D) where helium bubble growth occurs mainly by thermal SIA emission. This region was not found by Russell et al. [1–4], where they did not incorporate the thermal emission rate of SIAs into their model. However, the probability of forming helium bubbles in the region (D) is considered to be very small except relatively small helium bubbles at this equilibrium condition, because helium bubbles in the adjacent region (C) will go in a lower right direction and therefore paths to the region (D) could be quite limited. Thus, whether thermal SIA emission is included into the model (our model) or not (Russell's model), the nucleation paths of helium bubbles at the equilibrium condition are identical as described above.

4.6. Helium bubble growth and shrinkage during irradiation

The rates of inflow to a helium bubble and outflow from a helium bubble were separately calculated for vacancies, helium interstitials and SIAs at the irradiation condition at 800 K. The values of $X_V = 10^{-8}$, $X_{He} = 10^{-10}$ and $X_{SIA} = 6 \times 10^{-11}$ were used as $C_k(\infty)$ in Eq. (20). The mechanism map was obtained and is shown in Fig. 9(a) and (b).

The mechanism map at the irradiation condition is quite different from that at the equilibrium condition. A main difference between the two conditions is caused by a difference in the inflow rates of helium and SIAs. These point defects have high formation energy (~5 eV) and therefore they usually can not exist in the matrix at the equilibrium condition. However, at the irradiation condition, these defects can exist in the matrix because of their continuous production due to irradiation, which leads to a difference in the inflow rates between the two conditions.

The horizontal line that represents $N_{He}^b = \text{const.}$ in the mechanism map (Fig. 9) intersects the $J_{grow} = J_{shrink}$ line at (1) two different points unless N_{He}^b is so large and at (2) a single point when $N_{He}^b \sim 630$. In addition, there is (3) no intersection between the lines when $N_{He}^b > 630$. In the case of (1), helium bubbles which have the number of vacancies between the two intersections will shrink; and otherwise helium bubbles will grow. In the case of (3), on the other hand, all helium bubbles will grow. This dependence of growth and shrinkage behaviors on N_{He}^b is consistent with the void (bubble) growth rate curve of Mansur et al. [5–7].

From the mechanism map in Fig. 9, five regions are clearly defined as follows; (A) the region where helium bubbles may shrink mainly by thermal vacancy emission and helium may be absorbed, (B) the region where helium bubbles may shrink mainly by SIA absorption and helium may be absorbed, (C) the region where helium bubbles may grow by vacancy absorption and helium may be absorbed,

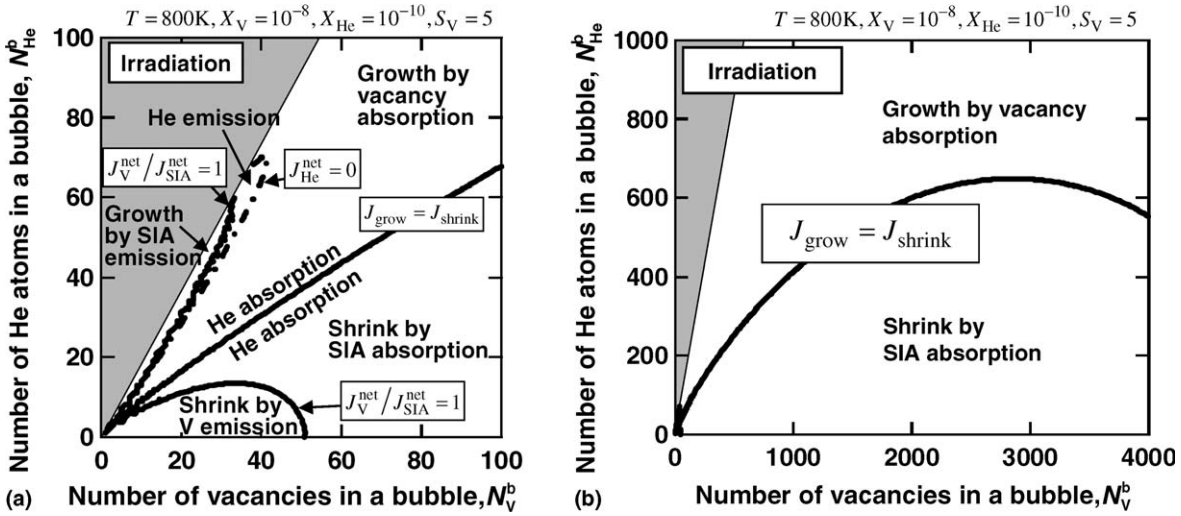

Fig. 9. A mechanism map for helium bubble nucleation and growth at the irradiation condition at 800 K. Matrix point defect concentrations are $X_V = 10^{-8}$, $X_{He} = 10^{-10}$, $X_{SIA} = 6 \times 10^{-11}$.

(D) the region where helium bubbles may grow mainly by vacancy absorption and helium is emitted, and (E) the region where helium bubbles may grow mainly by SIA emission and helium may be emitted. Note that the regions (D) and (E) overlap each other, where competitive reactions between the thermal emissions of helium and SIAs may occur.

Regarding the growth and shrinkage behaviors of helium bubbles, the mechanism map at the irradiation condition shows that the helium bubbles in both the regions (A) and (B) will go in an upper left direction, those in the region (C) will go in an upper right direction, and those in both the regions (D) and (E) will go in a lower right direction. Therefore, the nucleation paths of helium bubbles are shown by whole the region (C). Note that, different from the equilibrium condition mentioned above, the thermal emission of SIAs can be expected to occur, because the probability of forming helium bubbles in the region (E) cannot be ignored.

The actual nucleation paths of helium bubbles in the region (C) may depend on a balance between helium flow rate and helium bubble growth rate. Although the details of the actual trajectory of helium bubbles in the map must be obtained by solving the simultaneous rate theory equations as has done by Mansur et al. [5–7] and Stoller et al. [8,9], it is considered that helium absorption is a rate controlling reaction for helium bubble growth, when helium inflow rate is not enough and therefore helium bubbles go along near the $J_{grow} = J_{shrink}$ line. Such a rate controlling reaction may determine the incubation time of helium bubble growth.

In the present analysis the regions of helium emission and SIA emission appear near the region where He/V ratios are approximately around 2, which is near the application limitation of the linear elasticity theory. If the point defect binding free energy has the similar ratio dependence to the MD results as discussed in Section 4.1, it is considered that the regions of helium emission and SIA emission are appeared at the ratio of about 6. Analysis using the MD results is currently underway.

The present model describes all point defect emissions, but for simplicity it does not include defect cluster emissions. In order to more precisely solve the PSI problem, the rate of SIA cluster emission (loop punching) that can be evaluated using the binding energy of SIA clusters to a helium bubble [25], is required to be incorporated into the model. Furthermore, since the mechanism map shown here depends on temperature and total defect concentrations (X_V, X_{He} and X_{SIA}), more systematic analysis is required to understand the behaviors of helium bubble nucleation and growth at wider range conditions.

5. Conclusion

Free energy was evaluated for a system containing helium bubbles and point defects to understand helium bubble formation mechanism, available even at high helium concentration condition where

helium is directly implanted. The effect of helium on activation barrier for forming a helium bubble is clearly shown. In addition, the mechanism of helium bubble growth and shrinkage was discussed based on the inflow and outflow rates of point defects. It is emphasized that, at the irradiation condition investigated here, both the thermal emissions of helium and SIAs may competitively occur from a relatively small helium bubble with high helium pressure.

Acknowledgements

One of the authors (K.M.) would like to express his thanks to Dr W.G. Wolfer and his group for valuable discussion and encouragement during his visit to Lawrence Livermore National Laboratory. This work was supported in part by Japan–US joint research program (JUPITER-II) and by Kansai Research Foundation for technology promotion (KRF).

References

[1] K.G. Russell, Acta Metal. 19 (1971) 753.
[2] C.A. Parker, K.C. Russell, J. Nucl. Mater. 119 (1983) 82.
[3] C.A. Parker, K.C. Russell, Calculation of cavity nucleation under irradiation with continuous helium generation, in: H.R. Brager, J.S. Perrin (Eds.), Effects of Radiation on Materials: 11th Conference, ASTM STP 782, American Society for Testing and Materials, Philadelphia, 1982, p. 1042.
[4] K.G. Russell, Acta Metal. 26 (1978) 1615.
[5] L.K. Mansur, W.A. Coghlan, J. Nucl. Mater. 119 (1983) 1.
[6] L.L. Horton, L.K. Mansur, Experimental determination of the critical cavity radius in Fe–10Cr for ion irradiation, in: F.A. Garner, J.S. Perrin (Eds.), Effects of Radiation on Materials: 12th International Symposium, ASTM STP 870, American Society for Testing and Materials, Philadelphia, 1985, p. 344.
[7] W.A. Coghlan, L.K. Mansur, Effect of microstructure on the minimum critical radius and critical number of gas atoms for swelling, in: F.A. Garner, J.S. Perrin (Eds.), Effects of Radiation on Materials: 12th International Symposium, ASTM STP 870, American Society for Testing and Materials, Philadelphia, 1985, p. 481.
[8] R.E. Stoller, G.R. Odette, J. Nucl. Mater. 131 (1985) 118.
[9] R.E. Stoller, G.R. Odette, A comparison of the relative importance of helium and vacancy accumulation in void nucleation, in: F.A. Garner, N.H. Packan, A.S. Kumar (Eds.), Radiation-induced Changes in Microstructure: 13th International Symposium, ASTM STP 955, American Society for Testing and Materials, Philadelphia, 1987, p. 358.
[10] H. Iwakiri, K. Yasunaga, K. Morishita, N. Yoshida, J. Nucl. Mater. 283–287 (2000) 1134.
[11] J.H. Evans, A. van Veen, L.M. Caspers, Radiat. Effects 78 (1983) 105.
[12] H. Trinkaus, Radiat. Effects 78 (1983) 189.
[13] I.R. Brearley, D.A. MacInnes, J. Nucl. Mater. 95 (1980) 239.
[14] R.L. Mills, D.H. Liebenberg, J.C. Bronson, Phys. Rev. B 21 (1980) 5137.
[15] P. Vinet, J.R. Smith, J. Ferrante, J.H. Rose, Phys. Rev. B35 (1987) 1945.
[16] C.-S. Zha, H.-k. Mao, R.J. Hemley, Phys. Rev. B 70 (2004) 174107.
[17] A. Driessen, E. van der Poll, Phys. Rev. B 33 (1986) 3269.
[18] V.V. Kechin, J. Phys. Condens. Matter 7 (1995) 531.
[19] F. Datchi, P. Loubeyre, R.L. Toullec, Phys. Rev. B 61 (2000) 6535.
[20] D.A. Young, A.K. McMahan, M. Ross, Phys. Rev. B 24 (1981) 5119.
[21] F.E. Fujita, A theory of medium range order in supercooled liquid and amorphous solid metals, in: S. Steeb, H. Warlimont (Eds.), Rapidly Quenched Metals, Elsevier, Amsterdam, 1985, p. 585.
[22] G.J. Ackland, D.J. Bacon, A.F. Calder, T. Harry, Phil. Mag. A 75 (1997) 713.
[23] K. Morishita, B.D. Wirth, T. Diaz de la Rubia, A. Kimura, Effects of helium on radiation damage processes iron, in: S. Hanada, Z. Zhong, S.W. Nam, R.N. Wright (Eds.), Proceedings Fourth Pacific Rim International Conference on Advanced Materials and Processing (PRICM4), The Japan Institute of Metals, 2001, p. 1383.
[24] K. Morishita, R. Sugano, B.D. Wirth, T. Diaz de la Rubia, Nucl. Instrum. and Meth. B 202 (2003) 76.
[25] K. Morishita, R. Sugano, B.D. Wirth, J. Nucl. Mater. 323 (2003) 243.
[26] K. Morishita, R. Sugano, B.D. Wirth, Fusion Sci. Technol. 44 (2003) 441.
[27] J.D. Eshelby, The continuum theory of lattice defects, in: F. Seitz, D. Turnbull (Eds.), Solid State Phys., vol. 3, Academic, New York, 1956, p. 79.
[28] W.G. Wolfer, M. Ashkin, J. Appl. Phys. 46 (1975) 547.
[29] A. Seko, N. Odagaki, S.R. Nishitani, I. Tanaka, H. Adachi, Mater. Trans. 45 (2004) 1978.
[30] T. Kamijo, H. Fukutomi, Phil. Mag. A 48 (1983) 685.